Visual Neuroscience (2006), **23**, 115–126. Printed in the USA.

DOI: 10.1017/S0952523806231109

Receptive-field structure of optic flow responsive Purkinje cells in the vestibulocerebellum of pigeons

IAN R. WINSHIP[1] AND DOUGLAS R.W. WYLIE[1,2]

[1]Department of Psychology, University of Alberta, Edmonton, Alberta, Canada
[2]Centre for Neuroscience, University of Alberta, Edmonton, Alberta, Canada

(RECEIVED May 25, 2005; ACCEPTED November 23, 2005)

Abstract

Neurons sensitive to optic flow patterns have been recorded in the the olivo-vestibulocerebellar pathway and extrastriate visual cortical areas in vertebrates, and in the visual neuropile of invertebrates. The complex spike activity (CSA) of Purkinje cells in the vestibulocerebellum (VbC) responds best to patterns of optic flow that result from either self-rotation or self-translation. Previous studies have suggested that these neurons have a receptive-field (RF) structure that "approximates" the preferred optic flowfield with a "bipartite" organization. Contrasting this, studies in invertebrate species indicate that optic flow sensitive neurons are precisely tuned to their preferred flowfield, such that the local motion sensitivities and local preferred directions within their RFs precisely match the local motion in that region of the preferred flowfield. In this study, CSA in the VbC of pigeons was recorded in response to a set of complex computer-generated optic flow stimuli, similar to those used in previous studies of optic flow neurons in primate extrastriate visual cortex, to test whether the receptive field was of a precise or bipartite organization. We found that these RFs were not precisely tuned to optic flow patterns. Rather, we conclude that these neurons have a bipartite RF structure that approximates the preferred optic flowfield by pooling motion subunits of only a few different direction preferences.

Keywords: Optic flow, Vestibulocerebellum, Inferior olive, Optokinetic, Receptive fields

Introduction

As an organism moves through an environment consisting of numerous stationary objects and surfaces, characteristic patterns of visual motion occur across the entire retina. These patterns of motion are referred to as optic flow or flowfields (Gibson, 1954). Optic flowfields can be described as vector fields where the length of each vector gives the velocity and its orientation gives the direction of the respective image shift (Koenderink & van Doorn, 1987; Nakayama & Loomis, 1974; Krapp et al., 1998). The global structure of these flowfields depends on the type of self-motion being performed at a particular time. Fig. 1 shows examples of optic flowfields resulting from self-rotation (A) and self-translation (B & C), as projected onto a sphere surrounding the observer. Self-rotation produces a circular flow (opposite the direction of the head rotation) about the axis of rotation and laminar (planar) flow along the "equator" of this sphere. Self-translation also results in planar motion along the equator, but radial optic flow along the vector of translation. There is a focus of expansion (FOE; see Fig. 1C) in the direction of motion from which the visual image radiates outward and a focus of contraction (FOC) opposite the FOE where the visual image converges (see Fig. 1B).

In the vertebrate brain, neurons sensitive to optic flow patterns have been recorded in the the olivo-vestibulocerebellar pathway (e.g., Simpson et al., 1981; Leonard et al., 1988; Graf et al., 1988; Winship & Wylie 2001; Wylie et al., 1993, 1998), and extrastriate visual cortical areas, in particular the medial superior temporal cortex (MST) (Saito et al., 1986; Tanaka et al., 1986, 1989; Tanaka & Saito, 1989; Duffy & Wurtz, 1991*a*; for review, see Duffy, 2004). In the pigeon vestbulocerebellum (VbC), the complex spike activity (CSA) of Purkinje cells in the ventral uvula and nodulus is modulated best by optic flow that results from self-translation along one of three axes in three-dimensional space (Wylie et al., 1993, 1998; Wylie & Frost, 1999*a*). With respect to the preferred axes of translational optic flow, there are four relatively homogeneous response types organized into parasagittal zones (Wylie et al., 1998, 2003*b*; Wylie & Frost, 1999*a*). *Ascent* and *descent* neurons prefer flowfields resulting from upward or downward translation along the vertical axis. *Expansion* neurons respond best to optic flow resulting from forward translation along an axis oriented at 45 deg ipsilateral (i) to the midline and approximately +20-deg elevation (i.e., FOE at 45 deg i/+20-deg elevation) while *contraction* neurons prefer flowfields resulting from backward translation along an axis oriented at 45 deg contralateral (c) azimuth (FOC at 45 deg c azimuth). The preferred flowfields and

Address correspondence and reprint requests to: Douglas R. Wong-Wylie, Department of Psychology, University of Alberta, Edmonton, Alberta, Canada, T6G 2E9. E-mail: dwylie@ualberta.ca

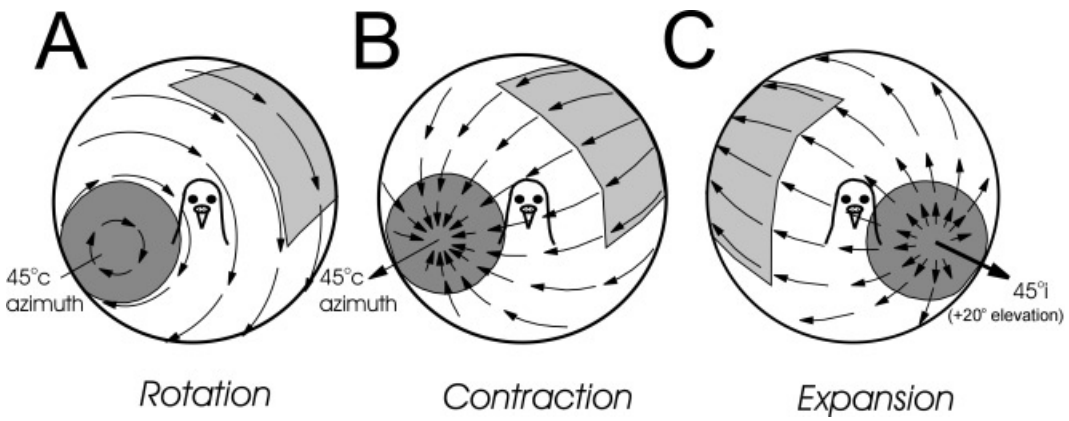

Fig. 1. Preferred optic flowfields for *rotation* (A), *contraction* (B), and *expansion* (C) neurons in the vestibulocerebellum (VbC). *Rotation* neurons prefer a circular flowfield rotating about an axis oriented at 45 deg c azimuth. *Contraction* neurons prefer radial optic flow with a focus of contraction (FOC) at 45 deg c azimuth. *Expansion* neurons prefer a radial optic flowfield with a focus of expansion (FOE) at 45 deg i/+20-deg elevation.

axes of translation are shown for *contraction* and *expansion* neurons in Figs. 1B and 1C, respectively. In the flocculus of the VbC, CSA responds best to optic flow resulting from self-rotation. The rotation cells in the flocculus respond best to rotational optic flow about one of two axes in three-dimensional space: either the vertical axis or an horizontal axis oriented at 45 deg c azimuth (Wylie & Frost, 1993). We refer to these two response types as *rVA* and *rH45c* neurons, respectively (Wylie, 2001; Winship & Wylie, 2001). The preferred flowfield and axis of rotation for an *rH45c* neuron is shown in Fig. 1A. In the rabbit VbC, *rVA* and *rH45c* neurons have been recorded (Leonard et al., 1988; Graf et al., 1988; Simpson et al., 1979, 1981, 1988*a*,*b*, 1989; Kano et al., 1990*a*,*b*; Kusunoki et al., 1990), but no translation-sensitive neurons have been found.

Simpson and colleagues (Leonard et al., 1988; Graf et al., 1988; Simpson et al., 1979, 1981, 1988*a*,*b*, 1989) suggested that the *rH45c* neurons were not precisely tuned to the rotational optic flowfield. Rather it was proposed that these neurons had a RF structure that "approximated" the preferred optic flowfield with a "bipartite" organization, as illustrated in Fig. 2E. The RF consists of a region preferring upward motion on the left apposed to a region preferring downward motion on the right. The preferred optic flowfield would be clockwise rotation about an axis centered on the boundary of the two hemifields. The bipartite RF structure contrasts with a RF structure that is "precisely" tuned to the preferred flowfield, which receives converging inputs from many direction-selective cells with small receptive fields (Tanaka et al., 1989; Orban et al., 1992; Krapp & Hengstenberg, 1996; Krapp et al., 1998). For example, a precisely tuned neuron preferring rotational optic flow would have a RF precisely matched to the flowfield shown in Fig. 2D: it would prefer rightward-downward motion in the shaded region S1, downward motion in S2, and upward-leftward motion in S3. Studies of optic flow sensitive neurons in primate MST and parietal cortex suggest that they have an underlying RF with precise tuning (Steinmetz et al., 1987; Tanaka et al., 1989; Tanaka & Saito, 1989; Orban et al., 1992; Duffy, 2004). To our knowledge, the stimuli used to show that the MST neurons do not have bipartite RFs have not been applied to the optic flow neurons in the olivo-cerebellar system.

Thus, in the present study, we investigated the RF structure of *expansion*, *contraction*, and *rH45c* neurons in the VbC of pigeons with two separate tests similar to those used in previous studies of extrastriate visual neurons (Tanaka et al., 1989; Tanaka & Saito, 1989; Schaafsma & Duysens, 1996). In general our results suggest that VbC neurons have an underlying bipartite receptive-field structure, as opposed to precise tuning.

Materials and methods

Surgery

The methods reported herein conformed to the guidelines established by the Canadian Council on Animal Care and were approved by the Biosciences Animal Care and Policy Committee at the University of Alberta. Silver King or Homing pigeons (*Columba livia*) were anesthetized with a ketamine (65 mg/kg)–xylazine (8 mg/kg) mixture (i.m.) and supplemental doses were administered as necessary. The animals were placed in a stereotaxic device with pigeon ear bars and beak adapter such that the orientation of the skull conformed to the atlas of Karten and Hodos (1967). A section of bone and dura was then removed to expose the cerebellum. Two different exposures were used: a medial exposure designed to access the ventral uvula and nodulus, and a lateral exposure through the anterior semicircular canal to access the flocculus.

Extracellular recordings and optic flow stimulation

Pigeons were removed from the ear bars and beak adapter after exposure of the cerebellum, and attached to a head bar such that their eye-beak angle was 34 deg, which is the normal orientation of the head in a freely moving bird (Erichsen et al., 1989). This involved pitching the beak upward about the interaural axis by 38 deg relative to the stereotaxic position of Karten and Hodos (1967). Extracellular single-unit recordings were then made using glass micropipettes filled with 2 M NaCl (tip diameters of 3–5 μm). Electrodes were advanced using an hydraulic microdrive (Frederick Haer & Co., Brunswick, ME) and raw signals were amplified, filtered, and fed to a data analysis system [Cambridge Electronic Designs (CED, Cambridge, UK) *1401plus*]. The raw trace of the extracellular recording was spike-sorted to ensure isolation of a

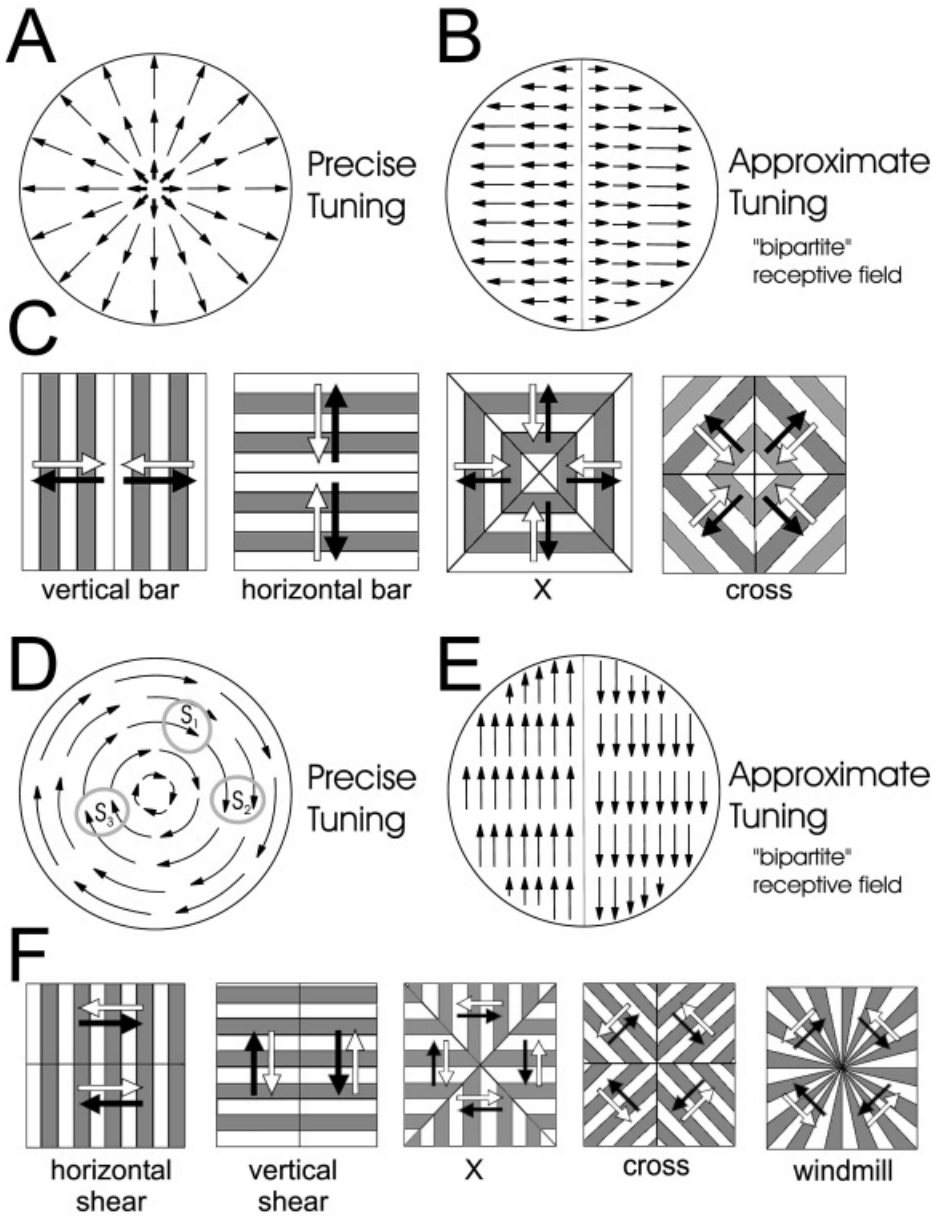

Fig. 2. Precise and approximate tuning of optic flow sensitive neurons in the vestibulocerebellum (VbC). A and B show how the response preferences of *expansion* neurons could be accounted for by precisely and approximately tuned receptive fields, respectively. D and E show precise and approximately tuned receptive fields for *rotation* neurons. C and F, respectively, show the composite stimuli used to test the receptive-field organization of translation-sensitive and *rotation* neurons in the VbC. The stimuli consisted of drifting square-wave gratings organized in such a way as to approximate the preferred flowfield around the preferred axis for an *expansion*, *contraction*, or *rotation* neuron.

single unit using *Spike2* software (CED). Peristimulus time histograms (PSTHs) were constructed using *Spike2*.

The CSA of Purkinje cells was identified and isolated based on their characteristic spike shape and spontaneous firing rate of about 1 spike/s. Isolated units were first stimulated with a large (about 90 deg × 90 deg) handheld stimulus consisting of a random pattern of dots and lines to determine if the cell was sensitive to visual stimulation. By moving this stimulus in different areas of the panoramic binocular visual field, the optic flow preference of each unit was qualitatively determined. On occasion we also recorded from the units in response to panoramic flowfields produced by planetarium projectors described in detail in previous studies (Wylie & Frost, 1993, 1999*b*). The test stimuli (see below) were back-projected onto a screen measuring 90 deg × 75 deg (width × height) that was positioned tangent to the preferred axis of translation or rotation for the isolated unit. The stimuli consisted of square-wave gratings (contrast = 0.80 [(LuminanceMAX-LuminanceMIN)/(LuminanceMAX+LuminanceMIN)]; mean luminance = 65 cd/m^2; refresh rate = 80 Hz) of an effective spatial and temporal frequency (spatial frequency = 0.25–0.5 cycles per degree (cpd), temporal frequency = 0.125–0.5 Hz; Winship et al., 2005).

Subfield stimuli

RF mapping studies in the parietal cortex of primates and in optic flow neurons in invertebrate species have typically utilized relatively small stimuli moving throughout the visual field to map visually responsive areas (e.g., *primates*, Schaafsma & Duysens, 1996; Duhamel et al., 1997; Ben Hamed et al., 2001; Bremmer et al., 2002; Avillac et al., 2005; *blowfly*, Krapp & Hengstenberg, 1996; Krapp et al., 1998; *shore crab*, Barnes et al., 2002). A larger stimulus was used in the present study, as small visual stimuli are not effective modulators of CSA in the VbC (Simpson & Alley, 1974). Thus, to determine the local motion sensitivity and local preferred direction in different areas of the RFs of *expansion*, *contraction*, and *rH45c* neurons (simply referred to as *rotation* neurons hereafter), 24 units were tested with a 45 deg × 37.5 deg square-wave grating drifting in different subfields. These eight subfields were centred about the preferred axis of rotation or translation (i.e., *rotation* units, 45 deg c; *expansion* units, 45 deg i/+20-deg elevation; *contraction* units, 45 deg c), and gratings of an effective spatial and temporal frequency were moved in eight directions (45° intervals) within each subfield to obtain a tuning curve for direction preference in each of the eight areas. Each sweep consisted of 2 s (s) of motion, a 1-s pause with a uniform grey screen of standard mean luminance, followed by 2 s of motion in the opposite direction, and a 1-s pause. Tuning curves were averaged from a minimum of six sweeps. The arrangement of the subfields is shown in Fig. 5A. Each subfield is identified numerically. For *rotation* and *contraction* units, subfields 1, 7, and 8 would span 45–90 deg c azimuth, and 3, 4, and 5 would span 0–45 deg c; for *expansion* units, subfields 3, 4, and 5 would span 45–90 deg i, and 1, 7, and 8 would span 0–45 deg i. Note that the subfields are overlapping. For example, subfield 2 includes the medial halves of subfields 1 and 3.

Vector analysis of subfield responses

The tuning curve for each subfield was assigned a vector illustrating the preferred direction and the breadth and magnitude of the direction selectivity. The preferred direction (*PD*) was calculated using the following equation:

$$PD = \tan^{-1}[(\Sigma\{(R_d)\sin(\theta_d)\})/(\Sigma\{(R_d)\cos(\theta_d)\})], \quad (1)$$

where θ_d is the direction of stimulus motion and R_d is equal to the firing rate minus spontaneous rate in response to that direction of stimulus motion.

Vector length was determined by calculating the sensitivity index (*SI*) for each tuning curve, as outlined by Vogels and Orban (1994). In circular statistics, the response R_d to each direction of motion is represented by a vector with a direction θ_d and length R_d. The *SI* represents the normalized length of the sum of these vectors:

$$SI = \{[\Sigma(R_d * \sin(\theta_d))]^2 + [\Sigma(R_d * \cos(\theta_d))]^2\}^{1/2}/(\Sigma R_d), \quad (2)$$

where R_d is equal to the firing rate minus spontaneous rate and θ_d is equal to the direction of stimulus motion. A higher *SI* reflects a narrower tuning curve. We then scaled the *SI* to the depth of modulation for that tuning curve, and these scaled *SI* values were then normalized among the eight subfields for each unit. In Fig. 5B, vectors representing the *PD* and scaled *SI* (vector length) are superimposed on their respective subfield tuning curves. In Fig. 6, the vectors from all subfields in 24 units tested with the subfield stimulus are illustrated according to cell type.

Composite large-field stimuli and rationale

Because CSA showed less than maximal modulation in response to the subfield stimuli, we also constructed composite large-field stimuli similar to those used in previous studies of MST (Tanaka et al., 1989; Tanaka & Saito, 1989) to directly test the bipartite versus precise RF structure predictions. These stimuli, illustrated in Figs. 2C and 2F, were composed of square-wave gratings drifting in different directions in different subregions of the RF, organized in such a way as to approximate the preferred flowfield along the axis of translation or rotation. *Expansion* neurons were tested using the stimulus illustrated in Fig. 2C centered to the axis at 45 deg i azimuth/+20-deg elevation (Wylie & Frost, 1999*a*; Winship & Wylie, 2001). The stimulus consisted of four configurations, each presented for 5 s with gratings moving centripetally (i.e., approximated contraction), followed by a 5-s pause with a uniform grey screen of standard mean luminance, 5 s of centrifugal motion (i.e., approximated expansion), and another 5-s pause. In the first two configurations (*horizontal bars* and *vertical bars*), the FOC/FOE was approximated using a bipartite stimulus with horizontal or vertical gratings moving in opposite directions. In the other two configurations (*X* and *cross*), the stimulus was divided into four subregions to more closely approximate the FOC/FOE. CSA modulation in response to each configuration was recorded over 3–10 sweeps. *Contraction* neurons were tested using the stimulus illustrated in Fig. 2C centred along the axis at 45 deg c azimuth.

Rotation neurons were tested using the stimulus illustrated in Fig. 2F centered along the axis at 45 deg c azimuth. The stimulus consisted of five configurations, each of which was presented for 5 s with clockwise (CW) movement of the gratings, followed by a 5.5-s pause with a uniform grey screen, 5 s of counterclockwise (CCW) motion, and another 5.5-s pause. Two configurations simulated rotational optic flow *via* a bipartite stimulus (*horizontal shear* and *vertical shear*), two conditions simulated rotation with a stimulus consisting of four subregions (*X* and *cross*), and a final condition projected a true rotational stimulus (*windmill*). CSA modulation in response to the stimulus was recorded over 3–10 sweeps. For units in the left flocculus, CW rotation would elicit maximal excitation, while CCW stimulus movement would inhibit the unit (neurons in the right flocculus showed the opposite direction preference).

Using these stimuli, the prediction was that if the RF were precisely tuned to their preferred optic flowfield, the CSA of translation-sensitive neurons would modulate equally to the *vertical bar* and *horizontal bar* conditions in Fig. 2C, and *rotation* neurons would modulate equally to the *horizontal shear* and *vertical shear* conditions shown in Fig. 2F. For example, if the response map along the preferred axis of an *expansion* neuron was precisely tuned to the preferred flowfield (i.e., the response map around the preferred axis precisely matched the flowfield as in Fig. 2A), an equal number of motion detectors would be excited by the *horizontal bar* and *vertical bar* conditions, and the neuron would show equal modulation to each condition (e.g., see Fig. 13 of Tanaka & Saito, 1989). Furthermore, modulation to the *X* and *cross* conditions should surpass that of the shear configurations since the *X* and *cross* more closely approximate the preferred flowfield (e.g., see Figs. 8 & 9 of Tanaka et al., 1989). However,

if the tuning was approximated using a limited number of direction preferences, such as illustrated in Fig. 2B, differential modulation to the two conditions would be expected. For a RF organized as in Fig. 2B, significant modulation to the *vertical bar* but not the *horizontal bar* configuration would be expected. For *rotation* neurons tested with the stimulus shown in Fig. 2F, the predictions would be nearly identical: if *rotation* neurons are precisely tuned, modulation to *horizontal shear* and *vertical shear* conditions should not differ, and more modulation might be expected to the *X*, *cross*, and *windmill* conditions which more closely approximate the flowfield around the axis of rotation (see Tanka & Saito, 1989; Tanaka et al., 1989).

Results

Experiments were performed in 19 pigeons. CSA in the VbC was isolated, and optic flow preference were reliably recorded and quantitatively identified as the *expansion, contraction*, or *rotation* response type. As in previous studies, we generally found several units of the same optic flow preference grouped into parasagittal bands in the VbC: *rotation* units were found laterally in the flocculus, while *contraction* neurons were found adjacent to the midline medial to *expansion* neurons in the nodulus and ventral uvula (Wylie et al., 1993; Crowder et al., 2000; Winship & Wylie, 2003; Wylie et al., 2003*a*,*b*). A total of 22 *rotation* units, 11 *expansion* units, and 22 *contraction* units were recorded and quantitatively analyzed in this study.

Responses to composite large-field stimuli

In Figs. 3A and 3B, we compare the responses of a *rotation* unit to the *vertical shear* stimulus (B) and panoramic optic flow about the preferred axis produced by a planetarium projector (A; see Wylie & Frost, 1993, 1999*a*). The depth of modulation in response to these two stimuli was virtually identical. In Fig. 3C, the modulation of a typical *rotation* unit in the right flocculus in response to all configurations of the simulated rotation stimulus is shown. White and black bars show the average firing rate of the unit minus spontaneous rate across five sweeps in response to simulated CW (white arrows) and CCW (black arrows) rotation, respectively. (Note: CW and CCW directions refer to the bird's perspective). The *horizontal shear* configuration resulted in very little modulation of this cell's CSA. All other conditions showed excitation in response to simulated CCW rotation, and inhibition to CW rotation. The *vertical shear* and *X* conditions produced the greatest modulation of CSA. Note the difference in modulation in the *horizontal shear* versus *vertical shear* conditions. Such a difference was present in all *rotation* units recorded in this study: *vertical shear* always resulted in much greater modulation than *horizontal shear*.

In Fig. 3D, the modulation of a typical *contraction* unit in response to all expansion/contraction configurations is illustrated. White and black bars, respectively, show the average firing rate of the unit minus spontaneous rate across six sweeps in response to simulated contraction (white arrows) and expansion (black arrows). Effectively no modulation occurred in response to the *horizontal bar* configuration, while in all other configurations, simulated contraction is preferred over expansion. The *vertical bar* condition showed the greatest modulation. In particular, note the difference in modulation in the *horizontal* versus *vertical bar* conditions. Such a difference was present in all *contraction* and *expansion* units recorded in this study: *vertical bars* always resulted in much greater modulation than *horizontal bars*.

Fig. 4A summarizes the responses of all *rotation* ($n = 22$) units. Depth of modulation was calculated for each of the five configurations using the following equation:

$$\text{Depth of Modulation} = (R_a - R_b)/(R_{\mathbf{a}} + R_b), \qquad (3)$$

where R_a and R_b, respectively, equal the firing rate to visual motion in the preferred and antipreferred directions. These values were then normalized among the five stimulus configurations (i.e., the stimulus configuration eliciting the greatest modulation was assigned a value of 1.0). The five resultant values were then averaged across all cells. *Horizontal shear* showed the least modulation of all configurations (0.303 ± 0.049, mean $\pm$ S.E.M.). Pair-wise comparisons (Tukey's HSD) showed that this value was significantly lower ($\alpha = 0.05$) than those for each of the other configurations (all $P \ll 0.001$). The depth of modulation for the *vertical shear* configuration was significantly greater than the *windmill* ($P < 0.002$), but not different from the *X* and *cross* configurations. The depth of modulation for the *X* configuration was significantly greater than all but the *vertical shear* configuration (*cross*, $P < 0.02$; *windmill*, $P \ll 0.001$). It is important to note that the depth of modulation in response to the *horizontal shear* configuration was significantly greater than 0 ($P < 0.001$)

Fig. 4B summarizes the response of all *contraction* ($n = 22$) and *expansion* ($n = 11$) units to the simulated contraction/expansion stimulus. As in Fig. 4A, the depth of modulation was calculated by averaging the normalized depth of modulation values for each of the four stimulus configurations [see eqn. (3)]. White and black bars show the mean depth of modulation for *contraction* and *expansion* units to each configuration, respectively. For the *contraction* units, *post-hoc* analysis using Tukey's HSD revealed that mean depth of modulation was significantly greater for the *vertical bar* configuration than all other configurations ($\alpha = 0.05$; *horizontal bar*, $P \ll 0.001$; *cross*, $P < 0.01$; *X*, $P < 0.002$). In addition, the depth of modulation values in response to the *horizontal bar* configuration was significantly less than all other configurations (*vertical bar*, $P < 0.000$; *cross*, $P < 0.001$; *X*, $P < 0.006$). For the *expansion* units, the depth of modulation was significantly different only for the *horizontal bar* versus *vertical bar* configurations ($P \ll 0.001$), although differences between the depth of modulation to the *vertical bar* versus the *X* and *cross* configurations approached significance ($P < 0.051$ and $P < 0.052$, respectively). Note that the *horizontal bar* configuration was significantly greater than 0 for both the *contraction* ($P \ll 0.001$) and *expansion* neurons ($P < 0.01$).

Responses to subfield stimulation

Twenty-four units (7 *rotation*, 11 *contraction*, 6 *expansion*) were tested with the subfield stimuli to determine the local motion sensitivity and direction preference in eight different subregions shown in Fig. 5A. Fig. 5B shows a representative series of tuning curves for a *rotation* cell. The tuning curves plot the firing rate minus spontaneous rate (areas in grey represent negative values) as a function of the direction of motion in polar coordinates, and the corresponding subfields are indicated numerically. For each tuning curve, vectors illustrating the preferred direction (*PD*) and scaled *SI* (as described in the Methods) are included. Based on these vectors, this neuron preferred downward motion in subfields 1 and 8, upward motion in subfields 3, 4, and 5, downward-rightward

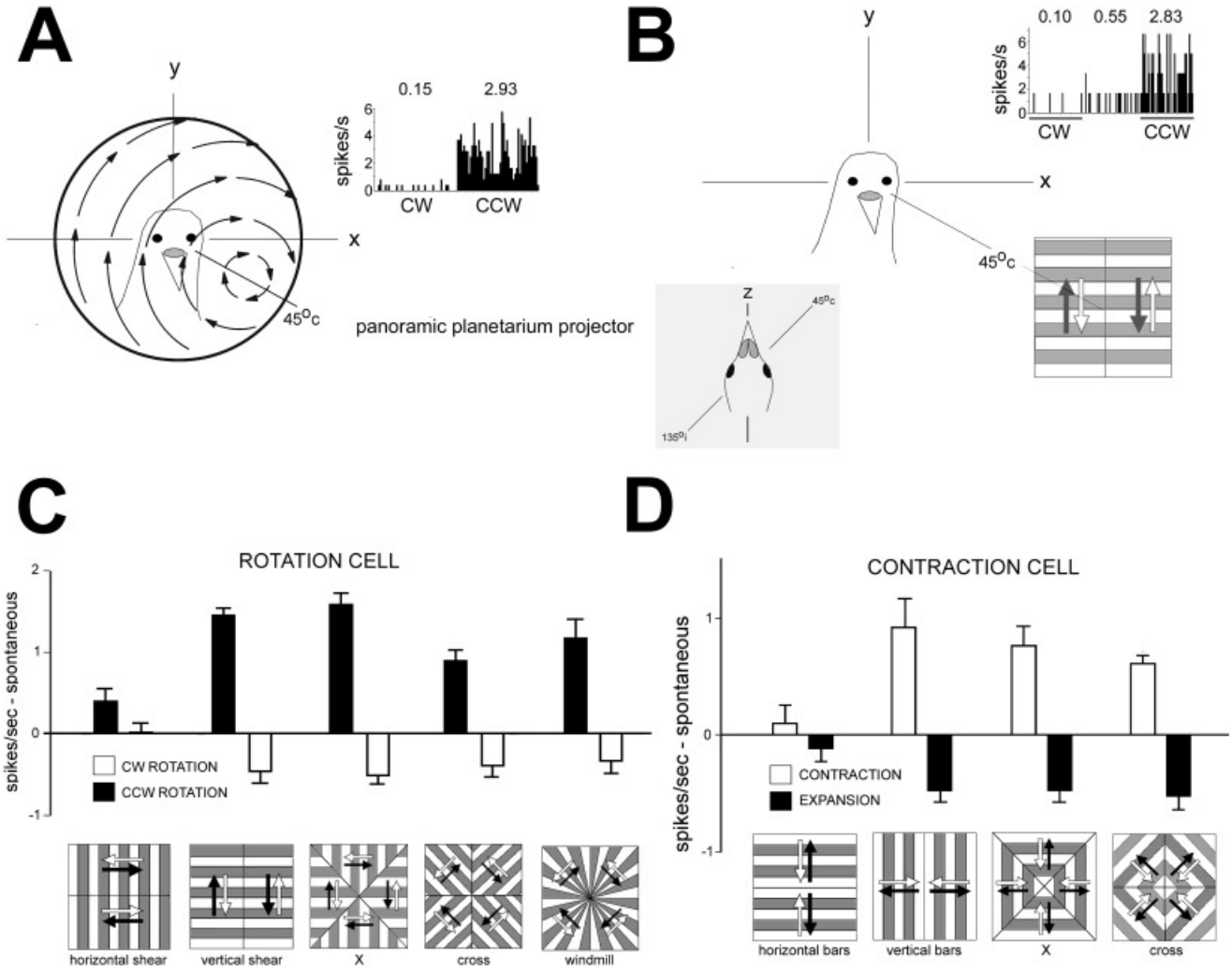

Fig. 3. A shows the modulation of a *rotation* unit in the right flocculus in response to the rotational optic flow about the preferred axis produced by a planetarium projector, recorded over 22 sweeps, where each sweep consisted of 5-s clockwise (CW) motion at a constant velocity of 2°/s, followed by 5-s of counterclockwise (CCW) motion. (Note, designation of CW or CCW rotation is from the bird's perspective). B shows the modulation of the same unit in response to the *vertical shear* configuration of the composite stimulus, recorded over six sweeps. Each sweep consisted of 5-s simulated CCW motion (generated by gratings moving upward from 0–45 deg c and downward from 45–90 deg c), a 5.5-s pause, followed by 5 s of simulated CW motion. The average firing rate (spikes/s) for each epoch is indicated above the histograms in A and B. Note that the modulation was about the same in response to both stimuli. C shows the firing rate of another *rotation* unit in the right flocculus in response to all configurations of the composite stimulus (depicted below the corresponding response). White and black bars show the average firing rate of the unit (minus spontaneous rate) in response to simulated CW (white arrows) and CCW (black arrows) rotation, respectively. D shows the firing rate of a *contraction* unit in response to all stimulus configurations. White and black bars show the average firing rate of the unit (minus spontaneous) in response to simulated contraction (white arrows) and expansion (black arrows), respectively, of the stimulus configuration shown directly below.

motion in subfield 7, and rightward motion in subfield 6. Clearly there were differences between the subfields with respect to the depth of modulation: greatest for subfields 1, 8, and 6 and least for subfields 2 and 3. In addition there were differences with respect to the breadth of tuning: clearly the cell was most tightly tuned to motion in subfield 1, and the tuning curve in subfields 2 and 7 were very broad.

The subfield tuning curves can be qualitatively examined to determine if they match a bipartite RF or a precisely tuned organization. For example, for the *rotation* unit shown in Fig. 5, the tuning curves in subfields 1 and 3 lend support to a bipartite RF organization; however, the tuning curves from subfields 5, 6, and 7 seem better aligned with a precisely tuned RF. Subfield 2 clearly does not support a precise RF structure. (Note, however, that the response observed in subfields 2 and 6 are difficult to determine. If the underlying receptive field is bipartite, the direction tuning for subfields 6 could be approximated by averaging the responses to fields 5 and 7).

In Fig. 6, vectors illustrating the *PD* and scaled *SI* of all subfield tuning curves are collapsed according to cell type. Dotted lines represent the mean preferred direction in each subfield as determined by vector summation, that is, the population response.

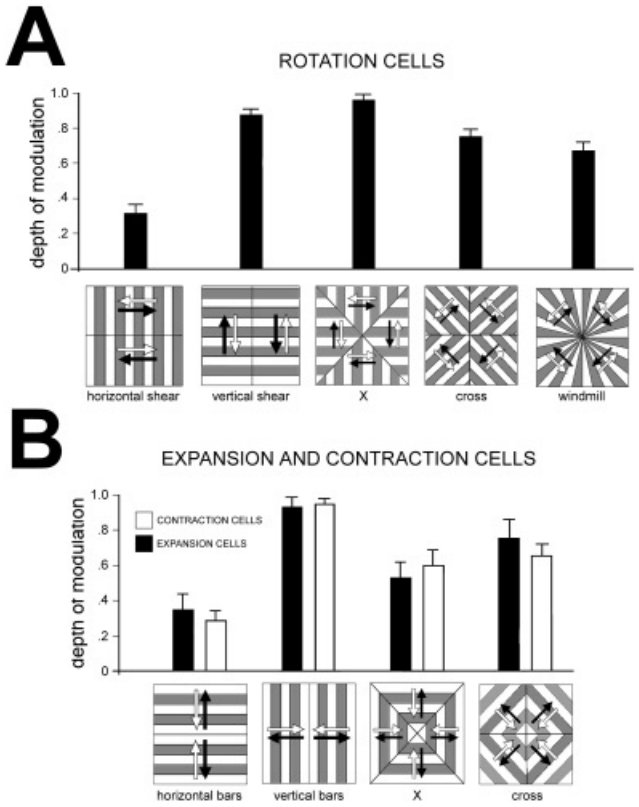

Fig. 4. A shows the normalized depth of modulation values for all *rotation* units ($n = 22$) in response to the composite stimulus configurations illustrated directly below. B shows the normalized depth of modulation values for all *expansion* ($n = 11$, black bars) and *contraction* ($n = 22$, white bars) units in response to the stimulus configurations illustrated directly below. A significant difference exists between modulation to *horizontal shear* versus *vertical shear* (A) and *horizontal bars* versus *vertical bars* (B).

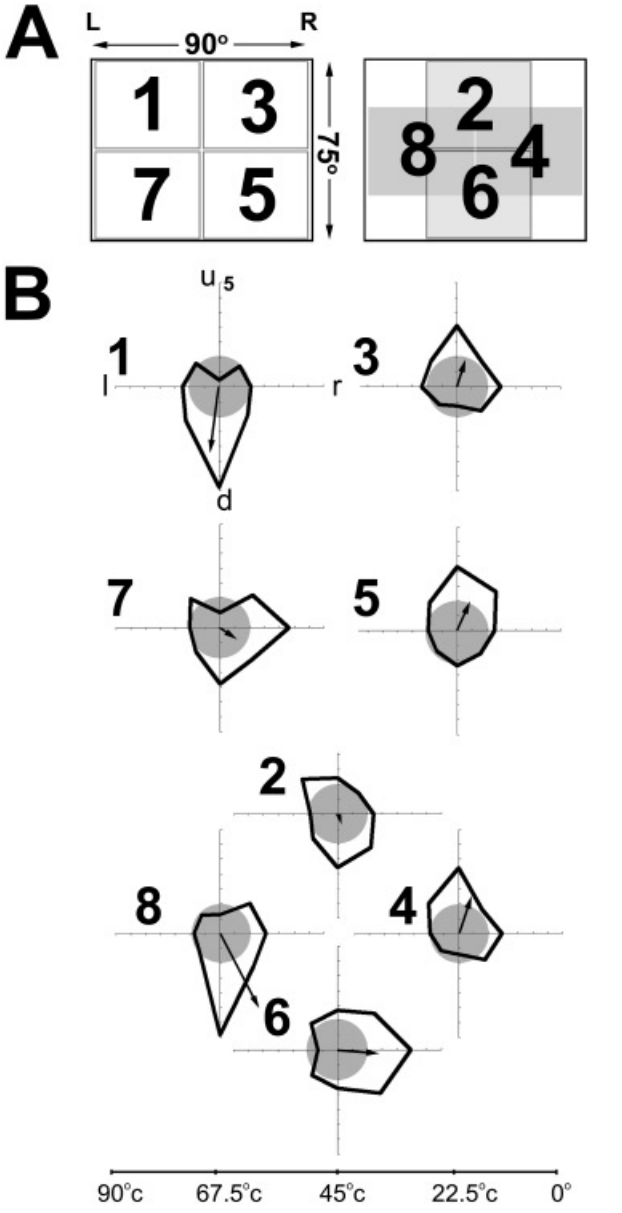

Fig. 5. A shows the eight subfields for which local tuning curves of *expansion*, *contraction*, and *rotation* were determined using drifting square-wave gratings. The screen was centred at 45 deg i/+20-deg elevation for *expansion* units and 45 deg c for *contraction* and *rotation* units. Local motion tuning curves for a representative *rotation* unit are shown in B. The polar plots show firing rate minus spontaneous rate, with grey shading representing negative values (i.e., inhibition). Arrows are vectors indicating the direction [*PD*, see eqn. (1)] and magnitude [scaled *SI*, see eqn. (2)] of the direction selectivity for a given subfield.

Solid and open circles, respectively, show the predicted preferred direction for each subfield in a bipartite or precisely tuned receptive field. Figs. 6A–6C show the vector fields for seven *rotation* units, 11 *contraction* units, and 6 *expansion* units, respectively. For Fig. 6A, qualitatively it appears that the population direction tuning is better approximated by the bipartite prediction. The data from fields 3, 5, and 7 show bias towards the precise predictions although the vector lengths are quite small. For field 6, the weighted average vector is close to the precise prediction, but the vectors are very small. For the *contraction* units (Fig. 6B), the vectors in subfields 1 and 3 appear closely aligned with the precise prediction, whereas fields 5 and 7 are closer to the bipartite prediction. Conversely, for the *expansion* units (Fig. 6C), the vectors in subfields 1 and 3 are closer to the bipartite prediction, whereas those in fields 5 to 7 are closer to the precisely tuned predictions.

To assess whether the bipartite or precisely tuned predictions offered a better estimate of true RF organization, a pair of quantitative analyses were performed. First, we calculated confidence intervals for the mean preferred angle *rotation*, *contraction*, and *expansion* units using a nonparametric bootstrap (Efron & Tibshirani, 1994). For each type of neuron, mean vectors from subfields 1, 3, 5, and 7 were reflected such that 0 deg would represent the bipartite prediction and 45 deg would be the precisely tuned prediction. Ninety-five percent confidence intervals (95% CI) for each class of neuron were then developed based on 1000 resamplings performed in *R* (*R* Development Core Team, 2005; see also Dalgaard, 2002). For the *contraction* units, the 95% CI for the mean is from −5.22 deg to 33.71 deg, while the 95% CI for means for *expansion* units was from −15.57 deg to 26.86 deg. Thus for *contraction* and *expansion* units, the 95% CI spanned the bipartite but not the precisely tuned prediction. For the *rotation* units, the 95% CI on means was from 6.58 deg to 26.55 deg, that is, did not

include either the bipartite or precise predictions, but was closer to the former.

A second quantitative analysis assessed the difference between the preferred direction for each cell in each subfield and the predicted preferred direction for a bipartite RF versus a precisely tuned RF (illustrated by the solid and open circles in Fig. 6, respectively). Bipartite predictions for fields 2 and 6 were obtained by averaging the tuning curves of the neighboring fields (1 and 3 for subfield 2, and 5 and 7 for field 6). The differences between the actual preferred directions and the predicted values were determined in each subfield, and a weighted average of each difference score was calculated for each unit across all subfields [using eqn. (2), where θ_d is the difference score from the bipartite or precise prediction for a given subfield and R_d is the scaled *SI* for that subfield]. Subfields 4 and 8 were not included in this analysis, as the predictions for a bipartite and precisely tuned RF are identical. Across all cell types, the mean difference score for the bipartite and precise predictions were 30.9 deg and 40.4 deg, respectively. These scores were significantly different (paired *t*-test, $\alpha = 0.05$; $P < 0.023$), suggesting the bipartite prediction is a better predictor of the RF organization. When analyzed by cell type, paired *t*-tests showed that the bipartite prediction was significantly closer to the actual preferred directions in *rotation* (18.3 deg *vs.* 35.1 deg; $P < 0.003$) and *expansion* (41.6 deg *vs.* 54.6 deg; $P < 0.048$) neurons. Difference scores for the bipartite versus precise predictions were not significantly different in *contraction* units (33.1 deg *vs.* 36.0 deg).

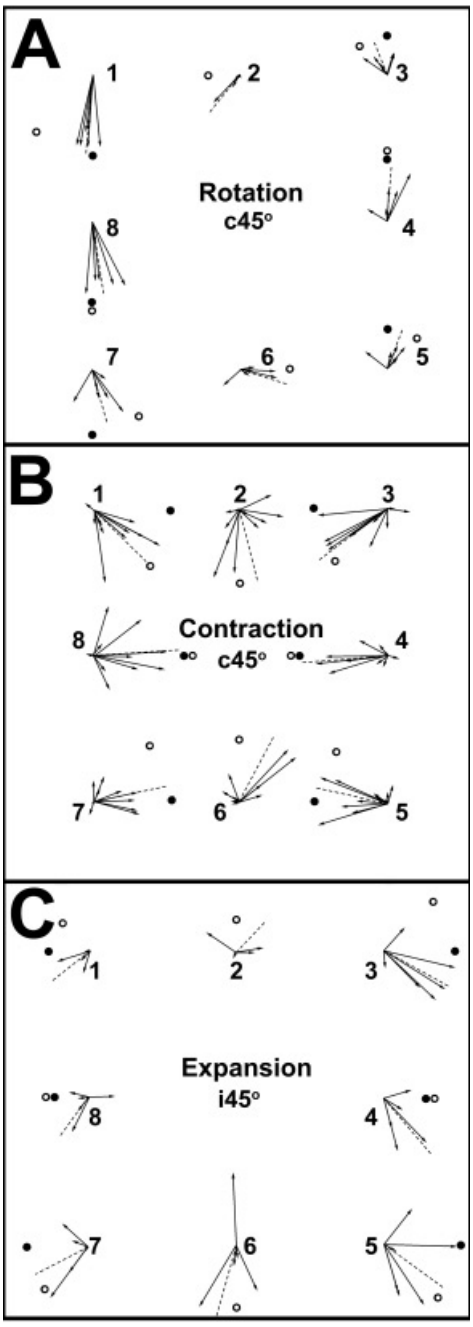

Fig. 6. Vector fields for *rotation*, *contraction*, and *expansion* units are shown in A, B, and C, respectively. The direction of the arrow is the *PD* [eqn. (1)] and vector length is equal to the scaled *SI* [eqn. (2)]. Each numeral 1–8 indicates the corresponding subfield, as defined in Fig. 5A. The dotted lines show the weighted-mean preferred direction for each subfield calculated using eqn. (1), where R_d and θ_d are the length and direction of each vector. Solid circles show the predicted preferred direction for each subfield in a bipartite RF (e.g., Figs. 2B & 2E), while open circles show the predicted preferred direction for a precisely tuned RF (e.g., Figs. 2A & 2D). Note that for subfields 4 and 8 the two predictions are coincident. For fields 2 and 6, a bipartite prediction was not indicated, since in a birpartite RF the tuning curve in this subfield would simply reflect an average of the neighboring subfields. Statistical analyses support a biparte RF organization moreso than a precise tuning.

Discussion

In this study, we examined the RFs of optic flow sensitive Purkinje cells in the VbC of pigeons to determine whether the RFs are precisely tuned to their preferred flowfield, as in invertebrate optic flow neurons, or represent coarse approximations of the flowfield, as had been suggested in the olivo-cerebellar system in mammals. Our results support the idea that the RF has a bipartite organization. However, we will argue that there might be a slight bias toward the precisely tuned model.

Responses to composite large field stimuli

Simpson and colleagues inferred the bipartite RF structure for the *rotation* neurons by noting that the rotation cells in the rabbit accessory optic system (AOS), inferior olive (IO), and VbC responded to upward motion on one side of the axis of preferred rotation, and downward motion on the other side of the axis (e.g., see Simpson et al., 1988*a*, Figs. 2 and 3; see also Kano et al., 1990*a*,*b*; Kusunoki et al., 1990). This has also been shown for the *rotation* neurons in the pigeon VbC and AOS (Wylie & Frost, 1993, 1999*b*; Wylie et al., 1993). However, it has been shown that cortical optic flow neurons with precise tuning still respond vigorously to such a stimulus (e.g., Fig. 13 of Tanaka & Saito, 1989). These neurons respond to shear about any axis, but the bipartite RF proposed by Simpson and colleagues (Fig. 2B) should not respond strongly to horizontal shear. As shown in Fig. 4A, for the *rotation* units the *vertical shear* configuration showed significantly greater modulation of CSA than the *horizontal shear* configuration. In fact, *horizontal shear* showed significantly less modulation

than all of the other stimulus configurations. For both *expansion* and *contraction* units, the *vertical bar* configuration produced significantly greater modulation of CSA than the *horizontal bar* configuration. These results argue strongly against precisely tuned RFs for optic flow sensitive neurons in the VbC of pigeons, and suggest that these neurons approximate the optic flowfield *via* a vertically divided bipartite RF, such as illustrated in Fig. 2B for an *expansion* neuron. However, there is one observation we would like to highlight that argues against a strict bipartite RF organization. For the *rotation* units, the depth of modulation to the *horizontal shear* configuration was significantly greater than zero, such that the response to simulated rotation in the preferred direction was greater than rotation in the opposite direction (see Fig. 4A). If the RF was organized as in Fig. 2E, one would not expect any modulation to this configuration. Likewise, for the *expansion* and *contraction* units, the depth of modulation to the *horizontal bar* configuration was significantly greater than zero (see Fig. 4B).

Subfield stimulation

To assess direction preference in different regions of the RF, we tested the response to subfield stimulation using drifting 45 deg × 37.5 deg square-wave gratings. A similar technique, albeit using smaller stimuli, has been used to assess the receptive-field structure of visual neurons in parietal cortex (Schaafsma & Duysens, 1996; see also Duhamel et al., 1997; Ben Hamed et al., 2001; Bremmer et al., 2002; Avillac et al., 2005). While the depth of modulation in response to this stimulation was not optimal, this allowed us to assign direction-tuning curves in eight regions of the RF around the FOE, FOC, or axis of rotation for *expansion*, *contraction*, and *rotation* units, respectively. Two statistical analyses of the local vector fields support a bipartite RF more so than a precisely tuned RF. The 95% CIs on the preferred directions for *expansion* and *contraction* units included the bipartite but not the precisely tuned prediction, while the 95% CI for *rotation* units included neither but was closer to the bipartite prediction. In addition, the disparity between the actual local tuning and the bipartite prediction was significantly less than the difference between actual data and the precisely tuned prediction. However, the spread of the vector fields is in the direction of the precisely tuned prediction, which suggests that the RF is biased towards a more precise tuning (e.g., Fig. 6A, subfields 3, 5, and 7; Fig. 6B, subfields 1 and 3; Fig. 6C, subfields 5 and 7). Furthermore, 95% CIs were not centered around the bipartite prediction but tended to bias towards the precise prediction.

Taken together, quantitative analyses of both the responses to the composite and subfield stimuli lend support to a bipartite organization. However, it would appear that the bipartite fields are biased towards a more precise organization than those illustrated in Figs. 2B and 2E.

Comparison to optic flow sensitive neurons in the MST of primates

Several groups have identified neurons in area MST and parietal cortex that respond to optic flow stimuli (e.g., Saito et al., 1986; Tanaka et al., 1986, 1989; Motter et al., 1987; Steinmetz et al., 1987; Tanaka & Saito, 1989; Duffy & Wurtz, 1991*a*,*b*, 1995; Orban et al., 1992; Lagae et al., 1994; Graziano et al., 1994; Schaafsma & Duysens, 1996; Page & Duffy, 2003; for review see Duffy, 2004). There are a wide variety of cortical optic flow neurons including neurons that show "position invariance" and those that prefer combinations of planar, radial, and circular optic flow (Duffy & Wurtz, 1991*a*,*b*, 1995; Graziano et al., 1994; Schaafsma & Duysens, 1996). Nonetheless, the underlying RF structure of cortical neurons responsive to expansion, contraction, and rotation has been investigated using stimuli similar to those employed in the present study, thus permitting a direct comparison of cortical and VbC optic flow neurons. Motter et al. (1987) and Steinmetz et al. (1987) stimulated contraction and expansion neurons area 7a of the primate parietal cortex with small visual stimuli moving throughout a neuron's RF. The population response of these neurons was precisely tuned to the local motion in their preferred flowfield (see Fig. 12 of Steinmetz et al., 1987). Tanaka and colleagues (Tanaka & Saito, 1989; Tanaka et al., 1989; see also Orban et al., 1992) stimulated expansion, contraction, and rotation neurons in MST with composite stimuli similar to those used in the present study. They approximated rotation, expansion, or contraction with composite stimuli constisting of two, four, or eight directions of motion, whereas we used stimuli consisting of two or four directions. Their results are in stark contrast to those of the present study. First, they found that rotation neurons responded much more strongly to true circular rotation than to shear along horizontal, vertical, or oblique axes. In contrast, we found that the response to vertical shear was significantly greater than that to true rotation (*windmill*, see Fig. 4A). Likewise, they found that expansion/contraction neurons responded much more strongly to true expansion/contraction as opposed to axial expansion/contraction, in which the radial motion was approximated with two subregions. Second, they found that the response increased as the number of directions in the composite stimuli increased from two to four to eight [see Figs. 8–11 from Tanaka et al. (1989)]. In fact only 5% of the neurons would respond significantly to the stimuli consisting of two directions. In contrast, for *rotation* neurons we found that the responses to the "*X*" and "*cross*" configurations were comparable or less than the response to *vertical shear*, and for *expansion* and *contraction* neurons the responses to the "*X*" and "*cross*" configurations were less than the responses to the *vertical bar* configuration (see Figs. 3 and 4). Finally for rotation neurons, Tanaka et al. (1989) showed that the responses to *vertical* and *horizontal shear* were essentially identical [see Fig. 13 of Tanaka & Saito (1989) and Fig. 8 of Tanaka et al. (1989)]. The reduced response to bipartite stimuli and the homogenous response to vertical and horizontal bipartite stimuli contrast with the response of optic flow neurons in the VbC from the present study. Based on the response properties of MST neurons described above, Tanaka et al. (1989) suggested that expansion, contraction, and rotation sensitive neurons might receive converging inputs from many directional cells in area MT with relatively small receptive fields in different parts of the visual field (termed the "mosaic" hypothesis). These receptive fields and direction preferences would have precise tuning to their preferred flowfield (see Fig. 12 of Tanaka et al., 1989). Orban et al. (1992) suggested that such an RF arrangement could account for position invariance and responses to multiple optic flow components.

Comparison to optic flow sensitive neurons in invertebrates

In the visual system of invertebrates, there are neurons responding to optic flow resulting from either self-rotation or self-translation (e.g., Krapp & Hengstenberg, 1996; Krapp et al., 1998; Barnes et al., 2002). Like neurons in the AOS, pretectum, and VbC, these optic flow cells are responsible for generating the optokinetic

response (Hengstenberg, 1993; Simpson, 1984). In blowflies and shore crabs, RF organization was assessed using intracellular recording in response to small moving visual stimuli (*blowfly*, Krapp & Hengstenberg, 1996; Krapp et al., 1998; *crab*, Barnes et al., 2002; Johnson et al., 2002), and it was determined that the RFs are precisely tuned to the preferred optic flowfield. Comparison to the present study is rather tenuous due to very different recording conditions and stimuli. Nonetheless, our results contrast the invertebrate studies. Thus, it appears that the RFs of optic flow neurons in the VbC of vertebrates are somewhat simplistic in their design compared to those in the visual neuropile of invertebrates. Also, it should be noted that despite the precisely tuned RF organization of the optic flow units in blowflies, these neurons are surprisingly broadly tuned to global rotational and translational optic flow patterns (Karmeier et al., 2003). In light of such broad tuning, a number of recent studies have emphasized the importance of the population code among optic flow sensitive neurons for the accurate assignment of direction of motion (Lappe et al., 1996; Ben Hamed et al., 2003; Page & Duffy, 2003).

Constructing bipartite receptive fields for expansion, contraction, and rotation

Simpson and colleagues originally conceived the notion of the bipartite receptive field as depicted in Fig. 2E for rotation neurons in the rabbit flocculus. For the rabbit VbC, the concept of the bipartite RF is consistent with (at least) two features of the physiology of the rabbit visual system. First, the visual input to the olivocerebellar pathway arises from the AOS (for reviews see Simpson 1984; Simpson et al., 1988*c*). These neurons have very large receptive fields, measuring at least 60 deg in diameter (Soodak & Simpson, 1988). Thus, the bipartite RF depicted in Fig. 2E could be constructed by pooling as few as two AOS neurons; one responsive to upward motion with one responsive to downward motion (Simpson, 1984; Simpson et al., 1988*b*). In contrast, a neuron with precise tuning would receive input from many units with smaller RFs (Tanaka et al., 1989; Krapp & Hengstenberg, 1996; Krapp et al., 1998; Barnes et al., 2002). Second, the rabbit retina has a streak organization and, according to Oyster et al. (1980), the density of ganglion cells that project to the AOS is highest in the visual streak. Thus, the bipartite RF depicted in Fig. 2E could arise from input from AOS cells preferring vertical motion along the visual streak, with little or no input from other areas of the retina.

A final feature of the AOS that is incompatible for constructing RFs that are precisely tuned is the fact that few directions are represented. Precise tuning requires input from neurons of many different direction preferences. In pigeons the visual input to the VbC originates in the nucleus of the basal optic root (nBOR) of the AOS and pretectal nucleus lentiformis mesencephali (LM). Homologous retinal recipient nuclei have been identified in mammals: the medial, lateral, and dorsal terminal nuclei of the AOS (MTN, LTN, and DTN, respectively) and the pretectal nucleus of the optic tract (NOT) (Fite, 1985; McKenna & Wallman, 1985; Simpson, 1984; Simpson et al., 1988*a*,*b*; Weber, 1985). Most AOS neurons prefer either upward, downward, or backward (nasal-temporal) visual motion, whereas most pretectal neurons prefer forward (temporal-nasal) motion (e.g., NOT, Collewijn, 1975*a*,*b*; Mustari & Fuchs, 1990; Ibbotson et al., 1994; LM, McKenna & Wallman, 1985; Winterson & Brauth, 1985; Wylie & Crowder, 2000; Wylie & Frost, 1996; MTN/LTN, Grasse & Cynader, 1982; Grasse et al., 1984; Soodak & Simpson, 1988; nBOR, Burns & Wallman, 1981; Rosenberg & Ariel, 1990; Wylie & Frost, 1990). Whole-cell patch recordings from the nBOR in turtles indicate that these neurons receive input from a few to several retinal subunits, each having approximately the same direction preference (Kogo et al., 1998).

Whereas the precursor direction cells for *expansion*, *contraction*, and *rotation* neurons in MST have small receptive fields, the AOS and pretectal precursors for olivo-cerebellar neurons have large receptive fields. The fact that pretectal and AOS neurons are tuned to the cardinal directions, rather than acting as motion detectors across the full spectrum of motion directions, provides a physiological base for the bipartite RFs in VbC. That is, our results suggest that bipartite receptive-field organization in the VbC may result from the pooling of relatively few precursor cells compared to optic flow neurons in MST. This is depicted in Fig. 7. In Fig. 7A, the bipartite RF of a *contraction* neuron is constructed *via* the juxtaposition of the RF of an LM cell selective for forward visual motion and the RF from an nBOR cell selective for backward visual motion on either side of the preferred axis at 45 deg c azimuth (i.e., a strict bipartite organization). In Fig. 7B, the RF of a *contraction* neuron is constructed using input from four neurons

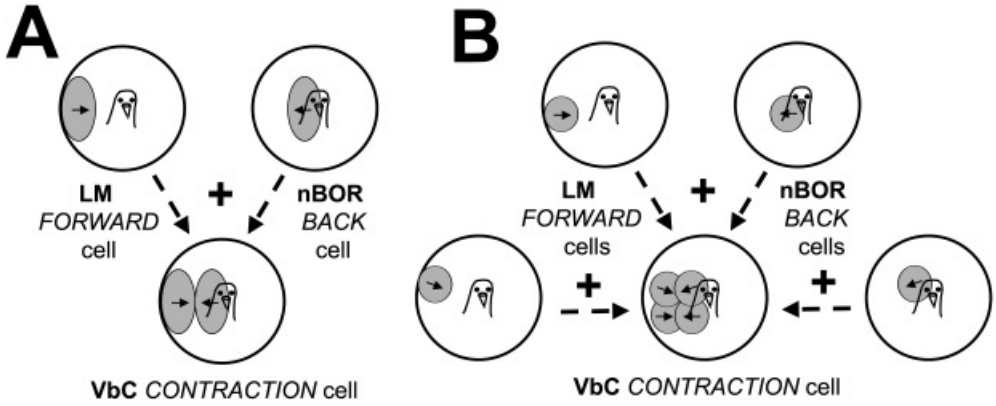

Fig. 7. In A, the receptive fields of a single direction selective unit in the pretectal nucleus lentiformis mesencephali (LM) and a single unit in the nucleus of the basal optic root (nBOR) of the accessory optic system (AOS) are combined to construct a strict bipartite receptive field of a *contraction* unit in the vestibulocerebellum (VbC). In B, four inputs are used to construct the receptive field of a *contraction* unit in the VbC.

in LM and nBOR, each with slightly different direction preferences and regions of peak excitability. Such a neuron would show a slight bias towards a precisely tuned RF organization.

Acknowledgments

We thank Peter L. Hurd for assistance with statistical analysis. This research was supported by funding from the Natural Sciences and Engineering Research Council of Canada (NSERC; to D.R.W.W.) D.R.W. Wylie was supported by the Canada Research Chairs Program. I.R. Winship was supported by scholarships from NSERC and the Alberta Heritage Foundation for Medical Research.

References

Avillac, M., Deneve, S., Olivier, E., Pouget, A. & Duhamel, J.R. (2005). Reference frames for representing visual and tactile locations in parietal cortex. *Nature Neuroscience* **8**, 941–949.

Barnes, W.J.P., Johnson, A.P., Horseman, B.G. & MacAuley, M.W.S. (2002). Computer-aided studies of vision in crabs. *Marine and Freshwater Behavioural Physiology* **35**, 1–2, 37–56.

Ben Hamed, S., Duhamel, J.R., Bremmer, F. & Graf, W. (2001). Representation of the visual field in the lateral intraparietal area of macaque monkeys: A quantitative receptive field analysis. *Experimental Brain Research* **140**, 127–144.

Ben Hamed, S., Page, W., Duffy, C. & Pouget, A. (2003). MSTd neuronal basis functions for the population encoding of heading direction. *Journal of Neurophysiology* **90**, 549–558.

Bremmer, F., Duhamel, J.R., Ben Hamed, S. & Graf, W. (2002). Heading encoding in the macaque ventral intraparietal area (VIP). *European Journal of Neuroscience* **16**, 1554–1568.

Burns, S. & Wallman, J. (1981). Relation of single unit properties to the occulomotor function of the nucleus of the basal optic root (AOS) in chickens. *Experimental Brain Research* **42**, 171–180.

Collewijn, H. (1975*a*). Direction-selective units in the rabbit's nucleus of the optic tract. *Brain Research* **100**, 489–508.

Collewijn, H. (1975*b*). Oculomotor areas in the rabbit's midbrain and pretectum. *Journal of Neurobiology* **6**, 3–22.

Crowder, N.A., Winship, I.R. & Wylie, D.R. (2000). Topographic organization of inferior olive cells projecting to translational zones in the vestibulocerebellum of pigeons. Journal of Comparative Neurology **419**, 87–95.

Dalgaard, P. (2002). *Introductory Statistics with R*. New York: Springer.

Duffy, C.J. (2004). The cortical analysis of optic flow. In *The Visual Neurosciences, Vol. 2*, ed. Chalupa, L.M. & Werner, J.S., pp. 1260–1283. Cambridge, Massachusetts: MIT Press.

Duffy, C.J. & Wurtz, R.H. (1991*a*). Sensitivity of MST neurons to optic flow stimuli. I. A continuum of response selectivity to large-field stimuli. *Journal of Neurophysiology* **65**, 1329–1345.

Duffy, C.J. & Wurtz, R.H. (1991*b*). Sensitivity of MST neurons to optic flow stimuli. II. Mechanisms of response selectivity revealed by small-field stimuli. *Journal of Neurophysiology* **65**, 1346–1359.

Duffy, C.J. & Wurtz, R.H. (1995). Response of monkey MST neurons to optic flow stimuli with shifted centers of motion. *Journal of Neuroscience* **15**, 5192–5208.

Duhamel, J.R., Bremmer, F., Ben Hamed, S. & Graf, W. (1997). Spatial invariance of visual receptive fields in parietal cortex neurons. *Nature* **389**, 845–848.

Efron, B. & Tibshirani, R.J. (1994). *Introduction to the Bootstrap*. New York: Chapman & Hall.

Erichsen, J.T., Hodos, W., Evinger, C., Bessette, B.B. & Philips, S.J. (1989). Head orientation in pigeons: Postural, locomotor, and visual determinants. *Brain, Behaviour, and Evolution* **33**, 268–578.

Fite, K.V. (1985). Pretectal and accessory-optic visual nuclei of fish, amphibia and reptiles: Themes and variations. *Brain, Behaviour, and Evolution* **26**, 71–90.

Gibson, J.J. (1954). The visual perception of objective motion and subjective movement. *Psychological Review* **61**, 304–314.

Graf, W., Simpson, J.I. & Leonard, C.S. (1988). Spatial organization of visual messages of the rabbit's cerebellar flocculus. II. Complex and simple spike responses of Purkinje cells. *Journal of Neurophysiology* **60**, 2091–2021.

Grasse, K.L. & Cynader, M.S. (1982). Electrophysiology of medial terminal nucleus of accessory optic system in the cat. *Journal of Neurophysiology* **48**, 490–504.

Grasse, K.L., Cyander, M.S. & Douglas, R.M. (1984). Alterations in response properties in the lateral and dorsal terminal nuclei of the cat accessory optic system following visual cortex lesions. *Experimental Brain Research* **55**, 69–80.

Graziano, M.S., Andersen, R.A. & Snowden, R.J. (1994). Tuning of MST neurons to spiral motions. *Journal of Neuroscience* **14**, 54–67.

Hengstenberg, R. (1993). Multisensory control in insect oculomotor systems. In *Visual Motion and Its Role in the Stabilization of Gaze*, ed. Miles, F.A., pp. 285–298. New York: Elsevier.

Ibbotson, M.R., Mark, R.F. & Maddess, T.L. (1994). Spatiotemporal response properties of direction-selective neurons in the nucleus of the optic tract and the dorsal terminal nucleus of the wallaby, *Macropus eugenii*. *Journal of Neurophysiology* **72**, 2927–2943.

Johnson, A.P., Horseman, B.G., MacAuley, M.W.S. & Barnes, W.J.P. (2002). PC-based visual stimuli for behavioural and electrophysiological studies of optic flow field detection. *Journal of Neuroscience Methods* **114**, 1, 51–61.

Kano, M., Kano, M.-S., Kusunoki, M. & Maekawa, K. (1990*a*). Nature of the optokinetic response and zonal organization of climbing fibre afferents in the vestibulocerebellum of the pigmented rabbit. *Experimental Brain Research* **80**, 238–251.

Kano, M., Kano, M.-S. & Maekawa, K. (1990*b*). Receptive field organization of climbing fibre afferents responding to optokinetic stimulation in the cerebellar nodulus and flocculus of the pigmented rabbit. *Experimental Brain Research* **82**, 499–512.

Karmeier, K., Krapp, H.G. & Egelhaaf, M. (2003). Robustness of the tuning of fly visual interneurons to rotatory optic flow. *Journal of Neurophysiology* **90**, 1626–1634.

Karten, H.J. & Hodos, W. (1967). *A Stereotaxic Atlas of the Brain of the Pigeon (Columba Livia)*. Baltimore, Maryland: Johns Hopkins Press.

Koenderink, J.J. & van Doorn, A.J. (1987). Facts on optic flow. *Biological Cybernetics* **56**, 247–254.

Kogo, N., McGartland Rubio, D. & Arial, M. (1998). Direction tuning of individual retinal inputs to the turtle accessory optic system. *Journal of Neuroscience* **18**, 2673–2684.

Krapp, H.G. & Hengstenberg, B. (1996). Estimation of self-motion by optic flow processing in single visual interneurons. *Nature* **384**, 463–466.

Krapp, H.G., Hengstenberg, B. & Hengstenberg, R. (1998). Dendritic structure and receptive-field organization of optic flow processing interneurons in the fly. *Journal of Neurophysiology* **79**, 1902–1917.

Kusunoki, M., Kan, M., Kano, M.-S. & Maekawa, K. (1990). Nature of optokinetic response and zonal organization of climbing fibre afferents in the vestibulocerebellum of the pigmented rabbit. I. The flocculus. *Experimental Brain Research* **80**, 225–237.

Lagae, L., Maes, H., Raiguel, S., Xiao, D.K. & Orban, G.A. (1994). Responses of macaque STS neurons to optic flow components: A comparison of areas MT and MST. *Journal of Neurophysiology* **71**, 1597–1626.

Lappe, M., Bremmer, F., Pekel, M., Thiele, A. & Hoffman, K.P. (1996). Optic flow processing in monkey STS: A theoretical and experimental approach. *Journal of Neuroscience* **16**, 6265–6285.

Leonard, C.S., Simpson, J.I. & Graf, W. (1988). Spatial organization of visual messages of the rabbit's cerebellar flocculus. I. Typology of inferior olive neurons of the dorsal cap of Kooy. *Journal of Neurophysiology* **60**, 2073–2090.

McKenna, O.C. & Wallman, J. (1985). Accessory optic system and pretectum of birds: Comparisons with those of other vertebrates. *Brain, Behaviour, and Evolution* **26**, 91–116.

Motter, B.C., Steinmetz, M.A., Duffy, C.J. & Mountcastle, V.B. (1987). Functional properties of parietal visual neurons: Mechanisms of directionality along a single axis. *Journal of Neuroscience* **7**, 154–176.

Mustari, M.J. & Fuchs, A.F. (1990). Discharge patterns of neurons in the pretectal nucleus of the optic tract (NOT) in the behaving primate. *Journal of Neurophysiology* **64**, 77–90.

Nakayama, K. & Loomis, J.M. (1974). Optical velocity patterns, velocity-sensitive neurons, and space perception: A hypothesis. *Perception* **3**, 63–80.

Orban, G.A., Lagae, L., Verri, A., Raiguel, S., Xiao, D., Maes, H. & Torre, V. (1992). First-order analysis of optical flow in monkey brain. *Proceedings of the National Academy of Sciences of the U.S.A.* **89**, 2595–2599.

Oyster, C.W., Simpson, J.I., Takahashi, E.S. & Soodak, R.E. (1980).

Retinal ganglion cells projecting to the rabbit accessory optic system. *Journal of Comparative Neurology* **190**, 49–61.

Page, W. & Duffy, C. (2003). Heading representation in MST: Sensory interactions and population encoding. *Journal of Neurophysiology* **89**, 1994–2013.

R Development Core Team. (2005). *R: A language and environment for statistical computing*. R Foundation for Statistical Computing. Vienna, Austria. http://www.R-project.org.

Rosenberg, A.F. & Ariel, M. (1990). Visual-response properties of neurons in turtle basal optic nucleus in vitro. *Journal of Neurophysiology* **63**, 1033–1045.

Saito, H., Yukie, M., Tanaka, K., Hikosaka, K., Fukada, Y. & Iwai, E. (1986). Integration of direction signals of image motion in the superior temporal sulcus of the macaque monkey. *Journal of Neuroscience* **6**, 145–157.

Schaafsma, S.J. & Duysens, J. (1996). Neurons in the ventral intraparietal area of awake macaque monkey closely resemble neurons in the dorsal part of the medial superior temporal area in their responses to optic flow patterns. *Journal of Neurophysiology* **76**, 4056–4068.

Simpson, J.I. (1984). The accessory optic system. *Annual Review of Neuroscience* **7**, 13–41.

Simpson, J.I. & Alley, K.E. (1974). Visual climbing fiber input to rabbit vestibulo-cerebellum: A source of direction-specific information. *Brain Research* **82**, 302–308.

Simpson, J.I., Giolli, R.A. & Blanks, R.H. (1988*c*). The pretectal nuclear complex and the accessory optic system. Reviews of Oculomotor Research **2**, 335–364.

Simpson, J.I., Graf, W. & Leonard, C. (1981). The coordinate system of visual climbing fibres to the flocculus. In *Progress in Oculomotor Research*, ed. Fuchs, A.F. & Becker, W., pp. 475–484. Amsterdam: Elsevier.

Simpson, J.I., Graf, W. & Leonard, C. (1989). Three-dimensional representation of retinal image movement by climbing fiber activity. In *The Olivocerebellar System in Motor Control: Experimental Brain Research Supplement, Vol. 17*, ed. Strata, P., pp. 323–327. Heidelberg: Springer-Verlag.

Simpson, J.I., Leonard, C.S. & Soodak, R.E. (1988*a*). The accessory optic system of rabbit. II. Spatial organization of direction selectivity. *Journal of Neurophysiology* **60**, 2055–2072.

Simpson, J.I., Leonard, C.S. & Soodak, R.E. (1988*b*). The accessory optic system: Analyzer of self-motion. *Annals of the New York Academy of Sciences* **545**, 170–179.

Simpson, J.I., Soodak, R.E. & Hess, R. (1979). The accessory optic system and its relation to the vestibulocerebellum. *Progress in Brain Research* **50**, 715–724.

Soodak, R.E. & Simpson, J.I. (1988). The accessory optic system of rabbit. I. Basic visual response properties. *Journal of Neurophysiology* **60**, 2055–2072.

Steinmetz, M.A., Motter, B.C., Duffy, C.J. & Mountcastle, V.B. (1987). Functional properties of parietal visual neurons: Radial organization of directionalities within the visual field. *Journal of Neuroscience*, **7**, 177–191.

Tanaka, K., Fukada, Y. & Saito, H.A. (1989). Underlying mechanisms of the response specificity of expansion/contraction and rotation cells in the dorsal part of the medial superior temporal area of the macaque monkey. *Journal of Neurophysiology* **62**, 642–656.

Tanaka, K., Hikosaka, K., Saito, H., Yukie, M., Fukada, Y. & Iwai, E. (1986). Analysis of local and wide-field movements in the superior temporal visual areas of the macaque monkey. *Journal of Neuroscience* **6**, 134–144.

Tanaka, K. & Saito, H. (1989). Analysis of motion of the visual field by direction, expansion/contraction, and rotation cells clustered in the dorsal part of the medial superior temporal area of the macaque monkey. *Journal of Neurophysiology* **62**, 626–641.

Vogels, R. & Orban, G.A. (1994). Activity of inferior temporal neurons during orientation discrimination with successively presented gratings. *Journal of Neurophysiology* **71**, 1428–1451.

Weber, J.T. (1985). Pretectal complex and accessory optic system in alert monkeys. *Brain, Behaviour, and Evolution* **26**, 117–140.

Winship, I.R., Hurd, P.L. & Wylie, D.R.W. (2005). Spatio-temporal tuning of optic flow inputs to the vestibulocerebellum in pigeons: Differences between mossy and climbing fibre pathways. *Journal of Neurophysiology* **93**, 1266–1277.

Winship, I.R. & Wylie, D.R.W. (2001). Responses of neurons in the medial column of the inferior olive in pigeons to translational and rotational optic flowfields. *Experimental Brain Research* **141**, 63–78.

Winship, I.R. & Wylie, D.R.W. (2003). Zonal organization of the vestibulocerebellum in pigeons (*Columba livia*): I. Climbing fibre input to the flocculus. *Journal of Comparative Neurology* **456**, 127–139.

Winterson, B.J. & Brauth, S.E. (1985). Direction-selective single units in the nucleus lentiformis mesencephali of the pigeon (*Columba livia*). *Experimental Brain Research* **60**, 215–226.

Wylie, D.R.W. (2001). Projections from the nucleus of the basal optic root and nucleus lentiformis mesencephali to the inferior olive in pigeons (*Columba livia*). *Journal of Comparative Neurology* **429**, 502–513.

Wylie, D.R.W., Bischof, W.F. & Frost, B.J. (1998). Common reference frame for neural coding of translational and rotational optic flow. *Nature* **392**, 278–282.

Wylie, D.R.W., Brown, M.R., Barkley, R.R., Winship, I.R., Crowder, N.A. & Todd, K.G. (2003*a*). Zonal organization the vestibulocerebellum in pigeons (*Columba livia*): II. Projections of the rotation zones of the flocculus. *Journal of Comparative Neurology* **456**, 140–153.

Wylie, D.R.W., Brown, M.R., Winship, I.R., Crowder, N.A. & Todd, K.G. (2003*b*). Zonal organization of the vestibulocerebellum in pigeons (*Columba livia*): III. Projections of the translation zones of the ventral uvula and nodulus. *Journal of Comparative Neurology* **465**, 179–194.

Wylie, D.R. & Crowder, N.A. (2000). Spatiotemporal properties of fast and slow neurons in the pretectal nucleus lentiformis mesencephali in pigeons. *Journal of Neurophysiology* **84**, 2529–2540.

Wylie, D.R. & Frost, B.J. (1990). Binocular neurons in the nucleus of the basal optic root (nBOR) of the pigeon are selective for either translational or rotational visual flow. *Visual Neuroscience* **5**, 489–495.

Wylie, D.R. & Frost, B.J. (1993). Responses of pigeon vestibulocerebellar neurons to optokinetic stimulation: II. The 3-dimensional reference frame of rotation neurons in the flocculus. *Journal of Neurophysiology* **70**, 2647–2659.

Wylie, D.R.W. & Frost, B.J. (1996). The pigeon optokinetic system: Visual input in extraocular muscle coordinates. *Visual Neuroscience* **13**, 945–953.

Wylie, D.R.W. & Frost, B.J. (1999*a*). Complex spike activity of Purkinje cells in the ventral uvula and nodulus of pigeons in response to translational optic flowfields. *Journal of Neurophysiology* **81**, 256–266.

Wylie, D.R. & Frost, B.J. (1999*b*). Responses of neurons in the nucleus of the basal optic root to translational and rotational flowfields. *Journal of Neurophysiology* **81**, 267–276.

Wylie, D.R., Kripalani, T.-K. & Frost, B.J. (1993). Responses of pigeon vestibulocerebellar neurons to optokinetic stimulation: I. Functional organization of neurons discriminating between translational and rotational visual flow. *Journal of Neurophysiology* **70**, 2632–2646.